Two-Photon Microscopy: Shedding Light on the Chemistry of Vision†

Yoshikazu Imanishi,*,‡ Kerrie H. Lodowski,‡ and Yiannis Koutalos*,§

Department of Pharmacology, School of Medicine, Case Western Reserve University, Cleveland, Ohio 44106-4965, and Department of Ophthalmology, Medical University of South Carolina, Charleston, South Carolina 29425

Received May 30, 2007; Revised Manuscript Received July 18, 2007

ABSTRACT: Two-photon microscopy (TPM) has come to occupy a prominent place in modern biological research with its ability to resolve the three-dimensional distribution of molecules deep inside living tissue. TPM can employ two different types of signals, fluorescence and second harmonic generation, to image biological structures with subcellular resolution. Two-photon excited fluorescence imaging is a powerful technique with which to monitor the dynamic behavior of the chemical components of tissues, whereas second harmonic imaging provides novel ways to study their spatial organization. Using TPM, great strides have been made toward understanding the metabolism, structure, signal transduction, and signal transmission in the eye. These include the characterization of the spatial distribution, transport, and metabolism of the endogenous retinoids, molecules essential for the detection of light, as well as the elucidation of the architecture of the living cornea. In this review, we present and discuss the current applications of TPM for the chemical and structural imaging of the eye. In addition, we address what we see as the future potential of TPM for eye research. This relatively new method of microscopy has been the subject of numerous technical improvements in terms of the optics and indicators used, improvements that should lead to more detailed biochemical characterizations of the eyes of live animals and even to imaging of the human eye in vivo.

For several hundred years the light microscope has allowed the visualization of biological structures and processes invisible to the naked eye and has been instrumental in the development of biology and medicine. The combination of microscopy with fluorescent labeling and staining dramatically improved sensitivity, while the use of fluorescent indicators responsive to different biochemical properties opened to scientific investigation a vast range of features in living cells. Standard light and fluorescence microscopy, however, can give only a two-dimensional view of a specimen. So, it was with the advent of confocal microscopy that three-dimensional (3D)[1] resolution was achieved. The further introduction of two-photon microscopy has improved the 3D imaging of living tissues and has the potential to allow noninvasive study of biochemical processes in vivo.

In fluorescence microscopy, the excitation light is focused on a plane through the specimen, but excitation occurs along the whole path of the light beam and not only at the plane of focus. Ordinarily, the fluorescence collected by the detectors would include the emission from outside the plane of focus, thereby precluding 3D resolution. In confocal fluorescence microscopy, an adjustable pinhole aperture is placed in front of the detector(s) that serves to reject the fluorescence originating from outside the focal plane. By moving the plane of focus up and down through the specimen, a 3D view of the distribution of fluorescence is obtained. With proper optics (an objective lens of sufficiently high numerical aperture) the collected images have subcellular resolution. Because a significant amount of fluorescence is rejected, it is necessary to use an intense light source for excitation, such as a laser, to obtain an image within a reasonable time. Phototoxicity and fluorophore bleaching can sometimes present a significant problem for confocal microscopy, as the intense light is shone repeatedly through the specimen. Since 1990 (*1*), two-photon excitation microscopy has revolutionized the study of biological structure and function by exciting fluorophores in biological specimens through the simultaneous absorption of two infrared (IR) photons (Figure 1A). This is achieved by focusing an infrared laser beam on the specimen, so that the high concentration of photons at the focal plane substantially increases the probability of the simultaneous absorption of two photons by a molecule of the fluorophore. In TPM, the requirement of a high infrared light intensity necessitates the use of a laser (*1*, *2*).

† This work was supported by NIH Grant EY014850 to Y.K. and postdoctoral support from National Institutes of Health Training Grant T32-DK07319 to K.L.

* To whom correspondence should be addressed. Y.I.: phone, 216-368-5226; fax, 216-368-1300; e-mail, yxi19@case.edu. Y.K.: phone, 843-792-9180; fax, 843-792-1723; e-mail, koutalo@musc.edu.

‡ Case Western Reserve University.

§ Medical University of South Carolina.

[1] Abbreviations: AMD, age-related macular degeneration; CFP, cyan fluorescent protein; FCS, fluorescence correlation spectroscopy; FP, fluorescent protein; FRET, fluorescence resonance energy transfer; GABA, γ-aminobutyric acid; PA-FP, photoactivatable fluorescent protein; GFP, green fluorescent protein; IR, infrared; LRAT, lecithin: retinol acyltransferase; RPE, retinal pigment epithelial or retinal pigment epithelium; SHG, second harmonic generation; SHIM, second harmonic imaging microscopy; TET, tetracycline; TPEM, two-photon excitation microscopy; TPM, two-photon microscopy; YFP, yellow fluorescent protein; 3D, three-dimensional.

10.1021/bi701055g CCC: $37.00
Published on Web 08/03/2007

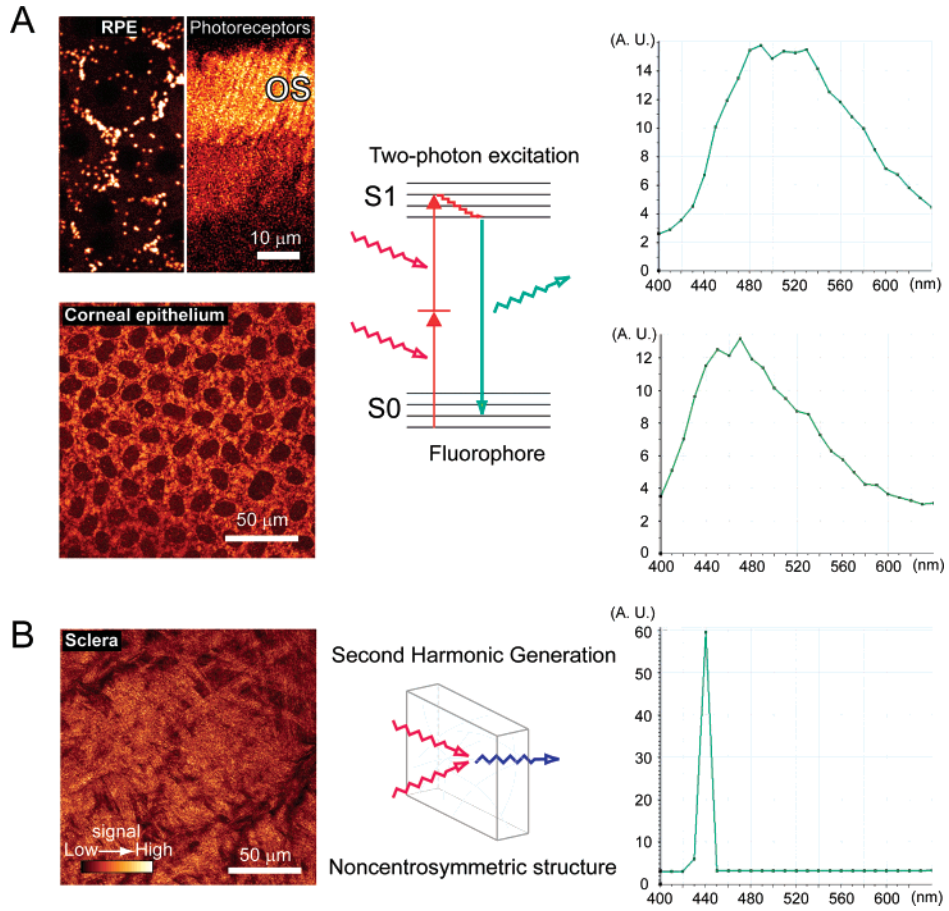

FIGURE 1: Two-photon imaging of structures in the mouse eye. (A) Left top panel: Images of two-photon excited fluorescence originating from retinyl esters in RPE cells (left) and retinol in rod photoreceptor outer segments (right, OS). Fluorescence was excited with 720−730 nm light from short-pulsed IR lasers. Left bottom panel: NAD(P)H in corneal epithelial cells was imaged by two-photon excitation at 730 nm. Middle panel: Schematic diagram of two-photon excitation of fluorescence; a single molecule of the fluorophore absorbs two photons simultaneously to reach an excited state. After a relaxation process, a single photon is emitted. Right panels: Fluorescence emission spectrum of the RPE cells (top) and the corneal epithelial cells (bottom). The *Y*-axis indicates the fluorescence intensity (arbitrary units), and the *X*-axis represents the wavelength of light. Note the broad fluorescence emission band. (B) Left panel: Second harmonic generation image from collagen structures in the sclera of an intact mouse eye. Illumination with 880 nm light from a short-pulsed IR laser. Middle panel: The process of second harmonic generation does not involve molecular excitation. A single photon is produced from the interaction of two photons with a noncentrosymmetric structure and without any energy loss. Right panel: The spectrum of the second harmonic signal from the sclera. The *Y*-axis indicates the intensity of the second harmonic signal (arbitrary units), and the *X*-axis represents the wavelength of light. Note the narrow band of the second harmonic signal peaking at 440 nm exactly half the wavelength of the incident light.

Two-photon excitation microscopy has two major advantages over conventional confocal laser scanning microscopy (Table 1 compares the characteristics of two-photon and confocal microscopy). First, the stimulating light beam has a high penetration depth because of the long (IR) wavelengths of light used; second, excitation takes place only at the plane of focus, due to the scaling of the probability of simultaneous photon absorption with the square of the local light intensity. Focal excitation avoids the simultaneous absorption of photons outside the imaging plane, thereby drastically reducing both phototoxicity and fluorophore bleaching. In combination with the high penetration depth, this has allowed imaging of live tissues and even of whole animals with high spatial resolution and over long periods of time. Moreover, because excitation and therefore emission take place only at the focal plane, it is unnecessary to place a pinhole aperture in front of the detector for the purpose of rejecting any scattered emitted light. Non-descanned detection without the aperture collects significantly more of the scattered emitted light, improving the signal-to-noise ratio severalfold and extending the imaging depth to several hundred micrometers (*3*−*5*). A drawback of non-descanned detection is that its spatial resolution is worse than that of conventional confocal microscopy. By using a descanned detector with an aperture placed in front, TPM can achieve a spatial resolution comparable to that of confocal microscopy (*3*, *5*), although this high resolution comes at the expense of the signal intensity.

At present, the spectrum of the typically used laser sources for TPM ranges from approximately 700 to 1100 nm, which would excite most of the relevant fluorophores, as their absorption spectra range from about 350 to 600 nm. The near-IR and red (600−700 nm) regions are considered to be the "optical window" of cells and tissues due to the lack of efficient endogenous one photon absorbers in this range (*6*). It is the presence of this "window", along with less scattering of the longer light wavelengths, that accounts for the deep tissue penetration of the two-photon excitation laser beam. Two-photon excitation has made a tremendous difference for the imaging of cellular autofluorescence, as this fluorescence derives mainly from UV-absorbing molecules such as the reduced pyridine nucleotides, NADH (reduced form of

Table 1: Comparison of Two-Photon and Confocal Microscopy[a]

features	two-photon microscopy	confocal microscopy
imaging depth	several hundred micrometers	less than TPM
spatial resolution	lower than that of confocal microscopy; resolution can be improved using a pinhole, however, at the expense of S/N ratio	high
S/N ratio	high; better than confocal microscopy if non-descanned detection is used	good
excitation/emission separation	wide (e.g., in the case of eGFP, 900−1000 nm excitation produces 510 nm peak emission)	close (e.g., in the case of eGFP, 488 nm excitation produces 510 nm peak emission)
excitation cross-talk in the presence of multiple fluorophores	difficult to preferentially excite a single fluorophore with two-photon stimulation	can reduce cross-talk by using different laser lines to preferentially excite particular fluorophores
imaging of UV absorbing fluorophores	deep tissue imaging is possible with infrared excitation because of less scattering and less absorption	imaging is possible with UV lasers, though with limited imaging depth; UV light is cytotoxic and subject to significant absorption and scattering within specimens
photobleaching and phototoxicity	limited to the focal point	through the whole light path of the laser in the specimen
imaging contrast	fluorescence, second harmonic generation; the IR beam can be used for single-photon reflection and transmission	fluorescence, reflection, transmission
lasers	IR pulsed (fs and ps) lasers; these lasers are more expensive and might require routine maintenance; fully automated, widely tunable lasers are commercially available	visible to UV range of CW (continuous wave) lasers; in general, the lasers for confocal microscopy are less expensive than the IR lasers used for TPM

[a] Each feature was compared qualitatively, because the quantifiable values, such as imaging depth and resolution, differ depending on the application and the tissue type. More comprehensive comparisons can be found in refs *5* and *122*.

nicotinamide adenine dinucleotide) and NADPH (reduced form of nicotinamide adenine dinucleotide phosphate), and in the case of the eye in particular vitamin A (all-*trans*-retinol). For such fluorophores, two-photon excitation circumvents the high phototoxicity and the limited penetration depth of UV light. In addition, imaging using two-photon excitation sidesteps the need for expensive optics optimized for UV excitation and suffers less from chromatic aberration problems (*5*).

Apart from the localized excitation of fluorescence, two-photon excitation can also be used for the localized release of "caged" compounds in living tissues and even in vivo. Such compounds include neurotransmitters (*7*), intracellular transmitters such as Ca^{2+} (*8*), or aqueous space tracers such as fluorescein (*9*), providing a powerful experimental tool for the fine manipulation of physicochemical processes and the spatial mapping of biochemical pathways in living tissues. In another important application, the same IR lasers can be used to elicit a second harmonic signal from molecules such as collagen, particularly useful for imaging the structure and organization of the extracellular matrix (*10*).

This review considers the applications of two-photon microscopy in vision research. The next section presents the types of indicators that can provide contrast for two-photon imaging, while the main section covers research advances in the biochemistry and architecture of the eye, as well as of signal transmission in the retina. The noninvasive character of two-photon imaging has made possible the study of biochemical reaction networks in the intact eye, without disrupting tissue integrity. For example, it has been of special significance for the study of the visual cycle, as this series of reactions that regenerates the visual pigment straddles two closely apposed cell types (photoreceptors and retinal pigment epithelial cells), and maintaining an intact tissue is imperative. In the last section we discuss emerging applications and what we consider important challenges for two-photon microscopy in the eye. One exciting possibility is that such noninvasive but high-resolution techniques will allow the study of the biochemical processes in the human eye in vivo and bring together basic and clinical research and diagnosis.

Indicators for Two-Photon Microscopy

The visualization of biological molecules and structures requires that they display a unique contrast compared to background. There are two main ways to produce contrast in two-photon microscopy, fluorescence and second harmonic generation. Because two-photon fluorescence and second harmonic generation are based on fundamentally different mechanisms (Figure 1), they can be used together to provide differential contrast in the imaging of tissue structure and function. Throughout the review, we use the term "two-photon microscopy (TPM)", collectively referring to two-photon excitation microscopy (TPEM) and second harmonic imaging microscopy (SHIM). A major advantage of this combinatorial imaging approach is that it can utilize endogenous fluorophores and structures without the addition of exogenous stains or extensive processing. Thus, the organization of the tissue can be examined with minimal perturbation, even in vivo. In this section we give an overview of the different indicator molecules, with an emphasis on applications relevant for the imaging of living eye tissues with two-photon microscopy.

(A) Fluorescent Indicators. Three types of fluorophores are of use in two-photon fluorescence microscopy of cells: endogenous fluorophores, fluorescent proteins, and exogenous fluorophores. A major class of endogenous fluorophores is composed of the intracellular molecules centrally involved in metabolic processes. These include NADH and NADPH, collectively referred to as NAD(P)H, and the oxidized forms of flavoproteins (*11*). Most of the NAD(P)H fluorescence originates from the mitochondria and can serve as the basis for redox fluorometry, a noninvasive optical method for monitoring cellular respiration (Figure 1A, bottom panels) (*12*, *13*). Apart from supplying the means for the functional imaging of metabolic activity, the fluorescence from pyridine nucleotides and flavins can also be used as

contrast for morphological imaging of living tissues. Other fluorophores of particular interest for the eye are retinol (vitamin A) and its fatty acid esters and lipofuscin. Lipofuscin is a complex fluorescent mixture of lipid and protein breakdown products that accumulates in granules of the retinal pigment epithelial cells (*14*). In the eye, TPEM of endogenous fluorophores has concentrated mostly on NAD(P)H and retinol and has been used for morphological imaging, for monitoring the metabolic state of cells, and for following the processing of retinol (Figure 1A).

Fluorescent proteins (FPs) are a key counterpart of TPEM for the imaging of biological structures and dynamic biochemical processes within whole living tissues (reviewed in ref *15*). FPs originate from the green fluorescent protein (GFP) discovered by Shimomura et al. (*16*). The chromophore of GFP is derived from the polypeptide chain through reactions involving cyclization, dehydration, and oxidation, so the protein does not require any exogenous cofactor to fluoresce (*15*). Biological applications of GFP-based fluorescent proteins exploded after its cloning and heterologous expression, as it allowed the engineering of proteins with a wide variety of properties. Today there are GFP variants with different excitation and emission spectra [for example, cyan fluorescent protein (CFP) and yellow fluorescent protein (YFP)], as well as enhanced fluorescence (eGFP, eCFP, eYFP) (*15*, *17*). Specially engineered variants can be selectively expressed in particular cell types, targeted to a specific organelle, used as protein tags, or modified so that their fluorescence becomes sensitive to pH, Ca^{2+}, and other ions (*15*, *18*). Finally, the construction of pairs of variants that can function as the donor and the acceptor for FRET (fluorescence resonance energy transfer) has created virtually unlimited possibilities for the optical study of cellular biochemistry. Clomeleon, a chloride ion sensor, is an example of a FRET-based sensor that has been used for studies of signal transmission in the retina (*19*). Clomeleon was made by fusing CFP (as the donor) and YFP (as the acceptor) via a short peptide linker. The quenching of YFP fluorescence by Cl^- results in changes of the FRET efficiency from CFP to YFP. More generally, FRET-based sensors rely on the steep dependence of the FRET signal on the distance between the donor and the acceptor. Such sensors can be used to monitor changes in a variety of intracellular molecules such as cAMP, cGMP, and inositol 1,4,5-trisphosphate (*18*, *20*). This is achieved by taking advantage of the conformational changes induced by such small molecules to an appropriate protein domain fused with a FP, as these changes would affect the distance between the donor and the acceptor. FPs appear quite promising for research in the retina, as their expression does not appear to affect morphology or function (*21*, *22*) and they can be efficiently excited with two-photon stimulation (*2*, *15*). They can be used to mark specific subpopulations of cells to enable their identification in the tissue during development or to tag specific proteins to allow the monitoring of their trafficking, targeting, and interactions within the cell. For signaling studies, mice expressing Cl^- and Ca^{2+} sensors in the retina under the control of the Thy-1 gene promoter (named because of its expression in thymocytes) or the tetracycline (TET) inducible promoter have been produced (*19*, *23*). Protein expression under the Thy-1 promoter labels a small population of cells, similar to Golgi stains, and is particularly useful for the imaging of individual neurons (*22*). The TET-regulated system, on the other hand, allows the temporal and spatial control of the expression of the sensor protein (*23*).

In spite of the tremendous advantages of FPs, especially in terms of targeting specificity and range of applications, a substantial amount of work is required to establish and maintain an animal line that expresses a particular FP. Thus, small exogenous fluorescent indicators and tracers are still indispensable tools for the study of biological structure, ionic concentrations, enzymatic activities, and membrane dynamics. For the optical monitoring of synaptic transmission, the charged styryl dyes, such as FM1-43 [*N*-(3-triethylammoniumpropyl)-4-[4-(dibutylamino)styryl]pyridinium dibromide], have been widely used as membrane markers (*24*) that become incorporated into synaptic vesicles through endocytosis. The loss of fluorescence accompanying release of the incorporated styryl dyes to the extracellular aqueous space serves as a measure of vesicle exocytosis and synaptic transmission.

(B) Second Harmonic Imaging Microscopy (SHIM) and Indicators. Structural molecules of the extracellular matrix, especially collagen, which is the most abundant structural protein in the human body, offer another way for imaging living tissues. Collagen and elastin emit enough fluorescence to provide contrast that in combination with the fluorescence of NAD(P)H has allowed the imaging of different layers of human skin in vivo with two-photon excitation microscopy (*25*). More importantly, however, and in addition to its fluorescence, collagen can give rise to a significant second harmonic signal (*26*). Significantly, the two-photon fluorescence and second harmonic collagen signals have been shown to correlate with the structural and mechanical properties of the collagen gel, opening a window to its biochemical properties (*27*). Apart from collagen, other structural protein assemblies, such as microtubules (*28*) and acto-myosin complexes (*29*), can give rise to large second harmonic signals. In the case of the eye, second harmonic imaging has been used to investigate the organization of the collagen in the cornea and the sclera (*30*−*36*) .

Second harmonic generation does not involve light absorption but rather the induction of a nonlinear polarization by the incident light that results in the production of photons at half the wavelength (*37*, *38*) (Figure 1B). As the amplitude of the second harmonic signal is proportional to the square of the incident light intensity, the resolution of SHIM is similar to that of TPEM. Because it does not involve absorption of the incident photons, second harmonic imaging does not suffer from photobleaching and phototoxicity. However, only molecules that lack a center of symmetry can give rise to a second harmonic signal. Moreover, and unlike fluorescence, which is emitted isotropically, the second harmonic signal is generally anisotropic. The angular distribution of the signal depends on the size and orientation of the scattering molecules as well as on the polarization of incident light (*39*). Under certain conditions, there is significant backward propagating second harmonic signal that could potentially be used for in vivo imaging (*38*).

Exogenous indicators can also be used for SHG studies with biological tissues, but they have to give rise to a noncentrosymmetric structure. Lipophilic molecules with high polarizability that accumulate preferentially to a mem-

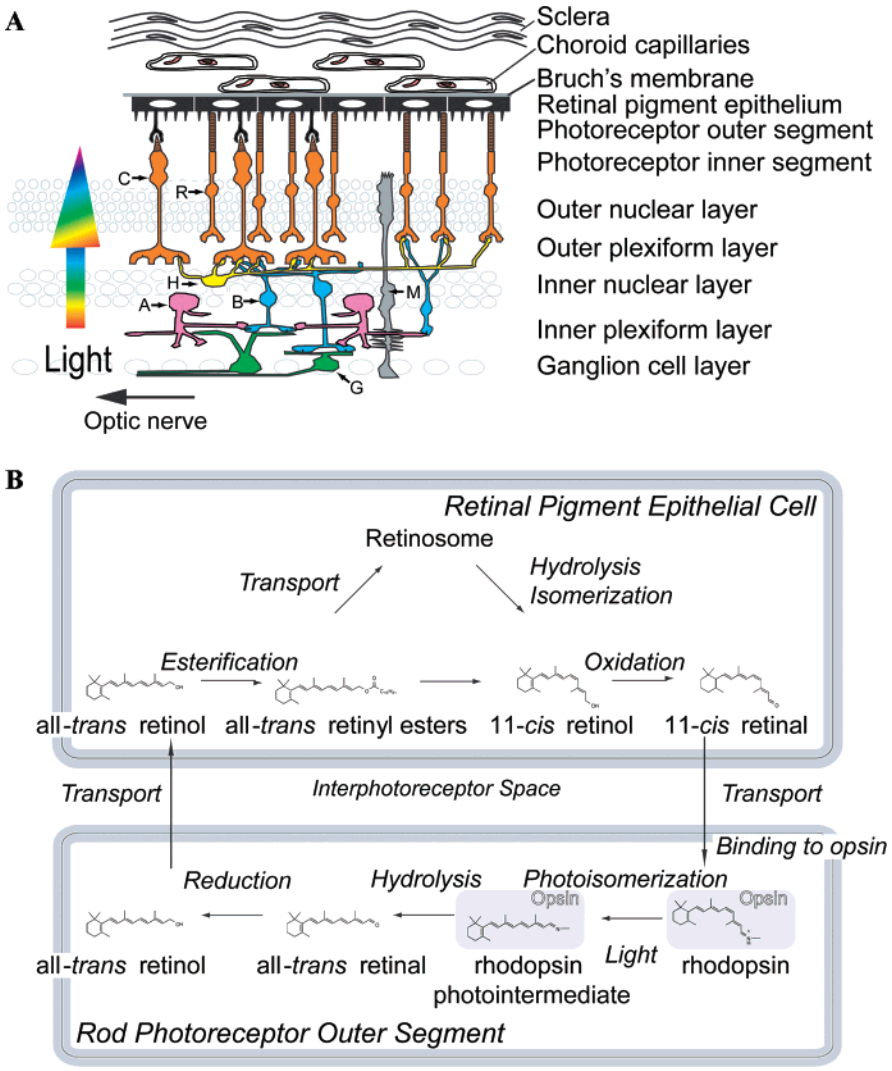

FIGURE 2: Architecture of the retina and the visual cycle. (A) Retina and surrounding structures. The retina is composed mainly of five types of neurons along with Müller glial cells (M) (*123*). A sixth type of neuron, the interplexiform cell that appears to carry information from the inner to the outer plexiform layer (*124*), is not shown. Rod (R) and cone (C) photoreceptors receive the light stimulus and convert it to an electrical signal. In the outer plexiform layer, photoreceptors form synapses with and pass the signal on to bipolar (B) cells. Bipolar cells pass on the signal to ganglion cells (G) either directly or through the amacrine cells (A) in the inner plexiform layer. The ganglion cell axons form the optic nerve that carries the signal to the brain. This vertical signal transmission is modulated through lateral connections by the horizontal (H) and amacrine (A) cells, which result in substantial visual signal processing within the retina. (B) Regeneration of 11-*cis*-retinal through the visual cycle. Light isomerizes the rhodopsin retinyl chromophore into an all-*trans* configuration. The chromophore is released and reduced in the rod outer segment to form all-*trans*-retinol. All-*trans*-retinol is transported to the retinal pigment epithelial cells, where it is esterified by LRAT. All-*trans*-retinyl esters are stored in the retinosomes and/or utilized for production of 11-*cis*-retinol through enzymatic hydrolysis and isomerization. Oxidation of 11-*cis*-retinol to retinal, the subsequent transport to rod outer segments, and binding to opsin complete the cycle.

brane leaflet can be used to provide contrast for morphological imaging (*40*). Moreover, as SHG has been shown to have intrinsic sensitivity to membrane voltage, such probes can be used for optical measurements of membrane potential as well (*41*, *42*). And by combining these probes with antibodies labeled with highly polarizable gold particles, SHG can be used to probe the membrane potential around single molecules (*43*).

Applications of Two-Photon Microscopy in Vision Research

(A) Retinoid Metabolism in the Eye. One of the areas of application of two-photon microscopy in the study of biochemical processes in the eye has been the fluorescence imaging of endogenous molecules involved in the visual process. A key molecule among these is vitamin A (all-*trans*-retinol), as well as its esters with fatty acids. The major role for vitamin A in the eye is to provide the chromophore of the visual pigment, the molecule responsible for the detection of incoming photons. The visual pigment is composed of a chromophore, 11-*cis*-retinal, covalently linked to a protein, opsin, and is concentrated in the outer segment compartment of the rod and cone photoreceptors, the cells responsible for the conversion of light to an electrical signal (Figure 2) (*44*, *45*). Absorption of a photon isomerizes the chromophore to all-*trans* and results in the production of an enzymatically active visual pigment intermediate that initiates a cascade of reactions leading to a change in the membrane potential of the photoreceptor cell (*46*). The photoisomerization of the chromophore, however, also results in the destruction of the visual pigment, and so its regeneration is necessary. The series of reactions that remake the visual pigment comprises

the visual cycle and, in the case of the rods, takes place within the photoreceptor outer segment and the adjacent retinal pigment epithelial (RPE) cells (Figure 2B; reviewed in refs *47*−*50*). First, within the outer segment of the photoreceptor cell, all-*trans*-retinal is released from the photoactivated pigment and reduced to all-*trans*-retinol by retinol dehydrogenase (*51*, *52*). All-*trans*-retinol is then transported to the RPE cells (*53*, *54*) where it is esterified by lecithin:retinol acyltransferase (LRAT) to form retinyl ester (*55*, *56*). The retinyl ester is isomerized and hydrolyzed by the RPE65 protein to 11-*cis*-retinol (*57*−*60*), which is oxidized to 11-*cis*-retinal (*61*, *62*). Inside the RPE cells 11-*cis*-retinal and retinol are carried by cellular retinaldehyde-binding protein (CRALBP) (*63*, *64*). 11-*cis*-Retinal produced in the RPE cells is then transported back to the photoreceptors where it re-forms the visual pigment. The regeneration of the pigment takes a long time for rod photoreceptors, which are responsible for vision at low light intensities. On the other hand, cone photoreceptors, which are responsible for vision at high light intensities, regenerate their pigment much faster, perhaps through the use of another pathway that involves the retinal Müller cells (M in Figure 2A) (*65*). Although the main pathway of the visual cycle has been well characterized thus far, questions remain about its regulation and maintenance under different light conditions, as well as about the interaction between different components and their cellular compartmentation. As mutations of several of the proteins involved in the cycle have been linked to hereditary blindness and degenerative diseases of the retina (*50*, *66*), the pathway is a potentially important target for pharmacological and therapeutic interventions.

Microscopy is an essential tool for understanding the flow of retinoids in relation to the underlying tissue architecture, and the fluorescence of endogenous fluorophores has been used to monitor the biochemical reactions of the visual cycle in living cells and eyes. In isolated photoreceptor cells, two compartments give rise to strong fluorescence signals upon excitation with UV light: the outer segment and the adjacent mitochondria-rich ellipsoid region (*67*, *68*). In dark-adapted photoreceptors, the outer segment fluorescence is very low, but there is a large increase following bleaching of the visual pigment. At the same time, the ellipsoid fluorescence shows only minor changes following light stimulation. Two-photon excitation of all-*trans*-retinol and NAD(P)H with 720 nm light from a Ti:sapphire laser has been used to measure the fluorescence emission spectra from the outer segment and the ellipsoid regions in isolated frog rod photoreceptors, demonstrating that the outer segment fluorescence originates from all-*trans*-retinol, while the ellipsoid fluorescence originates from NAD(P)H (*69*). Two-photon excitation of all-*trans*-retinol fluorescence and fluorescence recovery after photobleaching with 720 nm light has also been used to determine the mobility of all-*trans*-retinol in the outer segments of isolated rod photoreceptors, finding that all-*trans*-retinol in rod outer segments moves freely by passive diffusion (*70*). All-*trans*-retinol does not accumulate in the outer segments of photoreceptors in the intact living eye, as it is rapidly transported to the adjacent RPE cells (*71*). This rapid removal is not understood well, especially in view of the free diffusion of retinol in the rod outer segment. One possibility is that retinol is removed and transported by the interphotoreceptor retinoid binding protein (IRBP) (*72*), a retinoid-specific lipophilic carrier present in the interphotoreceptor matrix, and finally trapped in the RPE via esterification by LRAT.

RPE cells are required for generation and regeneration of the visual pigment chromophore and are known to store retinoids. Two-photon excitation microscopy of intact living eyes has identified specialized storage sites for retinyl esters, the retinosomes (*73*, *74*). Following illumination that bleaches the visual pigment, retinyl esters accumulate in the retinosomes, from where they are mobilized for the formation of 11-*cis*-retinol. Retinosomes are abundant in mice lacking the RPE65 isomerohydrolase protein, the enzyme that processes retinyl esters to form 11-*cis*-retinol (*73*). Compared to the photoreceptor outer segment, fluorescent retinoid species in the RPE are quite heterogeneous, including all-*trans*-retinol, 11-*cis*-retinol, all-*trans*-retinyl esters, and 11-*cis*-retinyl esters. A combination of TPEM and chemical analysis by HPLC identified all-*trans*-retinyl esters as the major source of fluorescence in retinosomes. The choroidal circulation provides another pathway for the supply of retinol to the RPE, delivering it through Bruch's membrane (Figure 2A). Impaired transport of retinol through a thickened Bruch's membrane may be responsible for diseases such as Sorsby fundus dystrophy that benefit from high oral doses of vitamin A (*75*). Retinol that is taken up from the choroidal circulation is also esterified by LRAT. Genetically modified mice lacking LRAT are deficient in this esterification process and do not exhibit retinosome fluorescence (*73*).

Defects in the flow of retinoids may play a significant role in a variety of degenerative diseases (*75*). Apart from monitoring the flow of retinoids, TPEM has also been used, albeit in a limited fashion, to track the processing of drugs used for pharmacological interventions. Thus, the fate of retinylamine, which has a long lasting inhibitory effect on the visual cycle that remains for several days even after a single administration (*76*), can be followed. Retinylamine, a specific blocker of 11-*cis*-retinal synthesis, is processed by LRAT to generate *N*-retinylamide that accumulates in the retinosomes (*77*). Such an approach is of course limited to fluorescing compounds like *N*-retinylamide.

In addition to retinol and retinyl esters, the posterior pole of the eye contains several other fluorescent substances (*78*). Granules containing lipofuscin, a fluorescent mixture of lipid and protein breakdown products, accumulate with age in the retinal pigment epithelial cells (*14*). A major fluorescent component of RPE lipofuscin is A2E, the product of the condensation of two all-*trans*-retinal molecules with phosphatidylethanolamine (*79*). A2E is cytotoxic (*80*), and its accumulation in the RPE has been linked to diseases such as Stargardt's that arise from defects in the processing of all-*trans*-retinal by the photoreceptor cells (*81*, *82*). The Bruch's membrane and sub-RPE deposits also exhibit substantial autofluorescence. Abnormal thickening of the Bruch's membrane and extensive accumulation of deposits are associated with the development of age-related macular degeneration (AMD) (*83*), the leading cause of blindness in industrialized countries (*84*). Significant differences in the fluorescence emission spectra of pigment epithelium, sub-RPE deposits between young and aged eyes have been observed with confocal and two-photon microscopy (*85*, *86*), paving the road for the use of imaging in the early diagnosis of eye pathologies.

(B) Redox Imaging of the Cornea. The cornea has long been the subject of metabolic studies utilizing redox fluorometry (*13*, *87*, *88*). Robust metabolism is essential for the maintenance of corneal transparency, which relies on the hydration state of the stroma layer (*89*−*91*). Two-photon excitation of NAD(P)H fluorescence can provide three-dimensional maps of the metabolic status of living rabbit cornea with subcellular resolution through the entire 400 μm thickness (*92*). Such resolution had been impossible to achieve with single-photon confocal microscopy (*93*).

(C) Architecture of the Cornea and Lens. The stromal layer of the cornea consists of ∼200 layers of collagen fibers, whose ordered structure gives the cornea its transparency (*89*, *90*). Second harmonic imaging of the sclera shows a more disordered state of the collagen fibers, consistent with its opaqueness (*30*). Analysis of second harmonic signals from the human cornea has identified three stroma layers with different patterns of collagen fiber packing (*94*) that is profoundly altered in corneas from patients with keratoconus (*34*, *36*), a disease associated with corneal thinning and conical shape formation (*30*, *34*, *36*). Mechanical interactions between collagen fibers and keratocytes (fibroblasts in the corneal stroma) play an essential role in the development of the highly organized collagen matrix. The collagen matrix is reorganized by fibroblasts during wound healing after corneal injury. To visualize this process in vivo, fibroblasts labeled with eGFP were introduced in injured rabbit corneas, and their repopulation was monitored in freshly excised corneal tissue with TPM (*95*).

Although the above studies were carried out with isolated corneas, ex vivo eyes, or in vitro cultured fibroblasts, second harmonic signals and two-photon excited fluorescence can be obtained from corneas in vivo through epidetection. SHIM holds significant promise for linking biochemical information on collagen structure with clinical diagnosis as it does not require any artificial labeling of the specimen.

Another area in which the particular advantages of two-photon microscopy are moving research forward is the structure and function of the lens (*96*). The lens is composed of a gradient of fiber cells at various stages of differentiation that are responsible for its structural organization and transparency (*89*). To maintain the optical transparency of the lens, it is necessary that the fiber cells exist in a regular geometric arrangement with minimal extracellular space so as to minimize discontinuities of refractive indices between them. In order to maintain the structural integrity and high transparency of the fiber cells in the absence of a blood supply, an internal circulation system exists that delivers nutrients and removes waste (*96*, *97*). The low chromatic aberration and the avoidance of extensive photobleaching of two-photon fluorescence microscopy have permitted the use of immunofluorescence to map with subcellular resolution the distribution of connexin-46, a gap junction protein, across large regions of the rat lens (*98*). The relationship between gap junction plaque distribution and intracellular communication was corroborated with photoactivation of caged fluorescein by two-photon excitation inside fiber cells. In the lens periphery, fluorescein moved radially, in an anisotropic manner, consistent with the location of the gap junction plaques on the broad sides of the cells in that region of the lens. Deep within the lens, fluorescein moved isotropically, consistent with the more uniform distribution of plaques there. Thus, the gap junctions constitute a part of the lens circulation system, and their distribution can sustain the radial movement of intracellular solutes between center and periphery (*96*, *98*).

(D) Functional Studies of Signal Transmission in the Retina. The retina contains mainly five types of neuronal cells (Figure 2A), all of which contribute in a unique way to the conversion and transmission of signals. Two-photon microscopy has specific advantages for the functional characterization of retinal neurons. First, the retina is particularly transparent to visible and IR light; therefore, the entire retina can be imaged with fluorescence at high spatiotemporal resolution. Second, as IR light is not efficiently absorbed by the rod and cone visual pigments, it can be used for two-photon excitation of fluorescent indicators without stimulating the photoreceptor cells (*99*). Intracellular and extracellular chemical signals can be visualized by fluorescence microscopy using the appropriate indicators, and TPEM has been used to resolve several specific questions about the transmission of the visual sensory signals through the retina.

In the retina, the first step of vision takes place in the outer segments of the rod and cone photoreceptor cells (R and C in Figure 2A), with the absorption of incident light by visual pigment molecules. In the absence of light, photoreceptor cells are partially depolarized and maintain a high release of the neurotransmitter glutamate from the synaptic terminal. Light absorption leads to hyperpolarization and a reduction in glutamate release. The photoreceptor cells then need to encode the light intensity received by the outer segments as the rate of release of glutamate-containing vesicles at the synaptic terminal. TPEM was used to characterize this encoding for cone photoreceptors in an intact lizard retina. The glutamate-containing vesicles at the synaptic terminals were loaded with the fluorescent tracer FM1-43, and the rate of vesicle release was measured from the rate of FM1-43 release at various light intensities (*100*). These measurements were put together with quantitative electron microscopy data, giving a vesicle release rate of 49 per 200 ms in the dark and dropping to 2 vesicles per 200 ms in bright light conditions. As cone cells operate over 4−5 log units of light intensity, these results show that cone cells compress 10 000-fold differences in light intensity into approximately 25-fold differences in output.

Photoreceptors form synapses with horizontal (H in Figure 2A) and bipolar (B in Figure 2A) cells. Bipolar cells are categorized into ON and OFF subtypes, depending on whether they hyperpolarize or depolarize, respectively, upon stimulation by glutamate from the photoreceptor cells. The response of the ON bipolar cells is modulated by γ-aminobutyric acid (GABA), released by the horizontal cells upon their stimulation by glutamate. The ON bipolar cells depolarize in response to GABA, but the mechanism had been difficult to establish experimentally. The technical obstacles were overcome with the use of TPEM and the ratiometric Cl^- indicator Clomeleon, expressed in subpopulations of mouse ON bipolar cells. The measurements demonstrated that in the ON bipolar cells there is an up to 20 mM higher Cl^- concentration in the dendrites than in the soma, and GABA application leads to Cl^- efflux from the dendrites, depolarizing the cell (*19*). TPEM is an essential tool for studying signaling involving dendritic processes, as they are

particularly fragile and difficult to target with microelectrodes and have to be studied in a tissue that has maintained the integrity of its neuronal circuitry. The capacity to study dendritic signaling has also been critical for experiments tackling the problem of motion detection, a fundamental property of visual perception. The signals received by the bipolar cells are transmitted to the amacrine (A in Figure 2A) and ganglion cells (G in Figure 2A) at the inner plexiform layer, where further signal processing occurs. Euler et al. used Ca^{2+} indicator dyes and TPEM in parallel with electrical recordings to demonstrate that in starburst amacrine cells, known to be essential for motion detection (*101*), it is the dendrites that respond to directional stimuli (*102*). Motion detection information is further processed and integrated by direction-sensitive ganglion cells. Two-photon Ca^{2+} imaging of ganglion cells showed that their dendrites are electrically excitable, triggering action potentials that further enhance the directional sensitivity of the cells (*103*).

Future Prospects

Presently, the application of TPM in the eye has led to important breakthroughs in the elucidation of retinoid processing in the retina and RPE and of collagen organization in the cornea. It has also shown tremendous potential for the understanding of visual signal transmission in the retina. The combination of two-photon excitation with other technologies holds great promise for the study of biochemical processes, while the noninvasive aspects of TPM are extending into clinical research and intervention. In this section we cover some of the potential avenues for future developments and applications.

One recent innovation is the development of photoactivatable and photoswitchable FPs (PA-FPs) (*104*). These proteins exhibit a large change in their fluorescence intensity or a shift in their excitation and emission spectrum upon absorption of light of particular wavelengths. PA-FP can be used to tag photoreceptor outer segment proteins, so that, in combination with two-photon photoactivation, their movements within the photoreceptor cell can be followed. This method will open new ways to approach long-standing questions about several photoreceptor processes, such as the targeting of phototransduction proteins and the massive light-induced translocation of outer segment components between different cellular compartments (*105*).

Two-photon excitation can also expand the range of fluorescence correlation spectroscopy (FCS) applications to include the study of biochemical processes within living cells. In FCS, a very small observation volume (~1 fL) that contains a small number of fluorescing particles is monitored over time. The measured fluorescence fluctuates as the particles move in and out of the observation volume or engage in chemical reactions. For a small number of particles the relative amplitude of fluctuations is quite large, and by analyzing the temporal fluctuations in fluorescence, one can obtain the number of particles, their diffusion coefficients, and the kinetic rate constants of biochemical reactions in which they participate (*106*, *107*).

Another important area is the development of three- and four-photon microscopy. In these cases, excitation involves the simultaneous absorption of three or four photons and would result in significantly higher 3D resolution, as excitation scales with the third or fourth power of the local light intensity. It will also open to exploration a host of additional pathways and cellular processes, as it allows the excitation of tryptophan and its indolamine derivatives that have single photon absorption maxima at less than 300 nm (*108*). An important hurdle that needs to be overcome is the need of at least an order of magnitude higher average laser power than TPM, because of the high intensities needed for efficient multiphoton absorption.

As we discussed previously, the low phototoxicity and high depth imaging of TPM are especially advantageous for research with intact living tissues and animals. They afford the opportunity to closely examine biochemical pathways such as the visual cycle and the response of animals to pharmacological interventions in vivo. The cellular underpinnings of the neuronal circuits of the retina, along with their development, can now be examined in detail with TPM in intact retinas or in vivo by marking particular cell types through the selective labeling by fluorescent proteins or dyes (*109*, *110*). And as the eye-specific depletion of gene function is not lethal, TPM is now coming to the forefront as a powerful tool for approaching the functional consequences of biochemical perturbations in animal models of human eye diseases (*111*−*113*). SHG offers an additional contrast mechanism that in combination with TPEM allows high-resolution imaging of extracellular and intracellular protein structures in living tissues (*10*). Second harmonic imaging can also utilize the polarization anisotropy of the SHG signal to probe the organization of such protein assemblies. Cell membranes, and their electrical potential, can also be visualized with second harmonic imaging through staining with lipophilic probes that accumulate preferentially to a membrane leaflet. Interestingly, retinal, the visual pigment chromophore, is one such highly polarizable molecule that can be used for imaging membrane potential (*114*).

Potential clinical applications of TPM are slowly emerging as well. For diagnostics, the autofluorescence and the second harmonic signal from the cornea appear to be most promising (*115*). They have already been used in animal studies for the noninvasive monitoring of corneal surgery in real time, with the same laser used for the imaging also used for cutting the tissue (*116*, *117*). Achieved by a multiphoton-mediated process, this kind of surgery can be highly precise, is essentially noninvasive, and can potentially avoid some of the tissue damage associated with other methods. Because of the relevance of the autofluorescence of the retina and the pigment epithelium for several degenerative diseases, the in vivo two-photon excitation microscopy of the human retina and pigment epithelium could become of tremendous diagnostic value. It will, however, need to overcome two important hurdles. One is the optical distortion caused by a human eye that results in diffusion of the focal spot (*118*) and reduces the efficacy of the two-photon process. Another is the large distance between the retina and the front of the eye, which limits the numerical aperture of the fundus ophthalmoscope for human eyes to approximately 0.2, much lower than the numerical aperture of >1.0 typically used for two-photon imaging of eyes in small animal models, such as mouse and zebrafish (*73*, *109*). The efficacy of two-photon excitation is dependent on the fourth power of the numerical aperture, and hence the two-photon process is estimated to be at least ~600 times less efficient for a human retina than

for that of small animals. Nevertheless, due to several technical advances (*5*, *119*−*121*), it is currently possible to optically compensate for some of the optical distortions, leading to improved image quality, penetration depth, and signal intensity and expanding the potential applications of TPM, at least for animals. Although still beyond our horizon, the development of a "two-photon ophthalmoscope" would make a dramatic difference in our ability to biochemically image the human eye in both normal and pathological conditions and be of major value for clinical diagnosis.

ACKNOWLEDGMENT

Y.I. thanks Dr. Krzysztof Palczewski for providing access to a two-photon microscope.

REFERENCES

1. Denk, W., Strickler, J. H., and Webb, W. W. (1990) Two-photon laser scanning fluorescence microscopy, *Science 248*, 73−76.
2. Svoboda, K., and Yasuda, R. (2006) Principles of two-photon excitation microscopy and its applications to neuroscience, *Neuron 50*, 823−839.
3. Schrader, M., Bahlmann, K., and Hell, S. W. (1997) Three-photon-excitation microscopy: theory, experiment and applications, *Optik 104*, 116−124.
4. Soeller, C., and Cannell, M. B. (1999) Two-photon microscopy: imaging in scattering samples, and three-dimensionally resolved flash photolysis, *Microsc. Res. Tech. 47*, 182−195.
5. Diaspro, A. (2002) *Confocal and Two-Photon Microscopy: Foundations, Applications, and Advances* (Diaspro, A., Ed.) Wiley-Liss, New York, NY.
6. Konig, K. (2000) Multiphoton microscopy in life sciences, *J. Microsc. 200*, 83−104.
7. Denk, W. (1994) Two-photon scanning photochemical microscopy: mapping ligand-gated ion channel distributions, *Proc. Natl. Acad. Sci. U.S.A. 91*, 6629−6633.
8. Lipp, P., and Niggli, E. (1998) Fundamental calcium release events revealed by two-photon excitation photolysis of caged calcium in Guinea-pig cardiac myocytes, *J. Physiol. 508* (Part 3), 801−809.
9. Soeller, C., Jacobs, M. D., Jones, K. T., Ellis-Davies, G. C., Donaldson, P. J., and Cannell, M. B. (2003) Application of two-photon flash photolysis to reveal intercellular communication, and intracellular Ca^{2+} movements, *J. Biomed. Opt. 8*, 418−427.
10. Campagnola, P. J., and Loew, L. M. (2003) Second-harmonic imaging microscopy for visualizing biomolecular arrays in cells, tissues and organisms, *Nat. Biotechnol. 21*, 1356−1360.
11. Huang, S., Heikal, A. A., and Webb, W. W. (2002) Two-photon fluorescence spectroscopy and microscopy of NAD(P)H and flavoprotein, *Biophys. J. 82*, 2811−2825.
12. Chance, B., and Thorell, B. (1959) Localization and kinetics of reduced pyridine nucleotide in living cells by microfluorometry, *J. Biol. Chem. 234*, 3044−3050.
13. Chance, B., and Lieberman, M. (1978) Intrinsic, fluorescence emission from the cornea at low temperatures: evidence of mitochondrial signals, and their differing redox states in epithelial, and endothelial sides, *Exp. Eye Res. 26*, 111−117.
14. Feeney-Burns, L., Hilderbrand, E. S., and Aging, S. (1984) Eldridge human RPE: morphometric analysis of macular, equatorial, and peripheral cells, *Invest. Ophthalmol. Visual Sci. 25*, 195−200.
15. Tsien, R. Y. (1998) The green fluorescent protein, *Annu. Rev. Biochem. 67*, 509−544.
16. Shimomura, O., Johnson, F. H., and Saiga, Y. (1962) Extraction purification, and properties of aequorin, a bioluminescent protein from the luminous hydromedusan, *Aequorea*, *J. Cell Comp. Physiol. 59*, 223−239.
17. Shaner, N. C., Steinbach, P. A., and Tsien, R. Y. (2005) A guide to choosing fluorescent proteins, *Nat. Methods 2*, 905−909.
18. Guerrero, G., and Isacoff, E. Y. (2001) Genetically encoded optical sensors of neuronal activity and cellular function, *Curr. Opin. Neurobiol. 11*, 601−607.
19. Duebel, J., Haverkamp, S., Schleich, W., Feng, G., Augustine, G. J., Kuner, T., and Euler, T. (2006) Two-photon imaging reveals somatodendritic chloride gradient in retinal ON-type bipolar cells expressing the biosensor Clomeleon, *Neuron 49*, 81−94.
20. Tanimura, A., Nezu, A., Morita, T., Turner, R. J., and Tojyo, Y. (2004) Fluorescent biosensor for quantitative real-time measurements of inositol 1,4,5-trisphosphate in single living cells, *J. Biol. Chem. 279*, 38095−38098.
21. Nour, M., Quiambao, A. B., Al-Ubaidi, M. R., and Naash, M. I. (2004) Absence of functional and structural abnormalities associated with expression of EGFP in the retina, *Invest. Ophthalmol. Visual Sci. 45*, 15−22.
22. Feng, G., Mellor, R. H., Bernstein, M., Keller-Peck, C., Nguyen, Q. T., Wallace, M., Nerbonne, J. M., Lichtman, J. W., and Sanes, J. R. (2000) Imaging neuronal subsets in transgenic mice expressing multiple spectral variants of GFP, *Neuron 28*, 41−51.
23. Hasan, M. T., Friedrich, R. W., Euler, T., Larkum, M. E., Giese, G., Both, M., Duebel, J., Waters, J., Bujard, H., Griesbeck, O., Tsien, R. Y., Nagai, T., Miyawaki, A., and Denk, W. (2004) Functional fluorescent Ca^{2+} indicator proteins in transgenic mice under TET control, *PLoS Biol. 2*, e163.
24. Betz, W. J., Mao, F., and Smith, C. B. (1996) Imaging exocytosis and endocytosis, *Curr. Opin. Neurobiol. 6*, 365−371.
25. Masters, B. R., So, P. T., Kim, K. H., Buehler, C., and Gratton, E. (1999) Multiphoton excitation microscopy, confocal microscopy, and spectroscopy of living cells, and tissues; functional metabolic imaging of human skin in vivo, *Methods Enzymol. 307*, 513−536.
26. Freund, I., Deutsch, M., and Sprecher, A. (1986) Connective tissue polarity. Optical, second-harmonic microscopy, crossed-beam summation, and small-angle scattering in rat-tail tendon, *Biophys. J. 50*, 693−712.
27. Raub, C. B., Suresh, V., Krasieva, T., Lyubovitsky, J., Mih, J. D., Putnam, A. J., Tromberg, B. J., and George, S. C. (2007) Noninvasive assessment of collagen gel microstructure and mechanics using multiphoton microscopy, *Biophys. J. 92*, 2212−2222.
28. Dombeck, D. A., Kasischke, K. A., Vishwasrao, H. D., Ingelsson, M., Hyman, B. T., and Webb, W. W. (2003) Uniform polarity microtubule assemblies imaged in native brain tissue by second-harmonic generation microscopy, *Proc. Natl. Acad. Sci. U.S.A. 100*, 7081−7086.
29. Campagnola, P. J., Millard, A. C., Terasaki, M., Hoppe, P. E., Malone, C. J., and Mohler, W. A. (2002) Three-dimensional high-resolution second-harmonic generation imaging of endogenous structural proteins in biological tissues, *Biophys. J. 82*, 493−508.
30. Teng, S. W., Tan, H. Y., Peng, J. L., Lin, H. H., Kim, K. H., Lo, W., Sun, Y., Lin, W. C., Lin, S. J., Jee, S. H., So, P. T., and Dong, C. Y. (2006) Multiphoton autofluorescence and second-harmonic generation imaging of the ex vivo porcine eye, *Invest. Ophthalmol. Visual Sci. 47*, 1216−1224.
31. Han, M., Zickler, L., Giese, G., Walter, M., Loesel, F. H., and Bille, J. F. (2004) Second-harmonic imaging of cornea after intrastromal femtosecond laser ablation, *J. Biomed. Opt. 9*, 760−766.
32. Lo, W., Teng, S. W., Tan, H. Y., Kim, K. H., Chen, H. C., Lee, H. S., Chen, Y. F., So, P. T., and Dong, C. Y. (2006) Intact corneal stroma visualization of GFP mouse revealed by multiphoton imaging, *Microsc. Res. Tech. 69*, 973−975.
33. Lyubovitsky, J. G., Spencer, J. A., Krasieva, T. B., Andersen, B., and Tromberg, B. J. (2006) Imaging corneal pathology in a transgenic mouse model using nonlinear microscopy, *J. Biomed. Opt. 11*, 014013.
34. Tan, H. Y., Sun, Y., Lo, W., Lin, S. J., Hsiao, C. H., Chen, Y. F., Huang, S. C., Lin, W. C., Jee, S. H., Yu, H. S., and Dong, C. Y. (2006) Multiphoton fluorescence and second harmonic generation imaging of the structural alterations in keratoconus ex vivo, *Invest. Ophthalmol. Visual Sci. 47*, 5251−5259.
35. Wang, B. G., Koenig, K., Riemann, I., Krieg, R., and Halbhuber, K. J. (2006) Intraocular multiphoton microscopy with subcellular spatial resolution by infrared femtosecond lasers, *Histochem. Cell Biol. 126*, 507−515.
36. Morishige, N., Wahlert, A. J., Kenney, M. C., Brown, D. J., Kawamoto, K., Chikama, T., Nishida, T., and Jester, J. V. (2007) Second-harmonic imaging microscopy of normal human and keratoconus cornea, *Invest. Ophthalmol. Visual Sci. 48*, 1087−1094.
37. Zoumi, A., Yeh, A., and Tromberg, B. J. (2002) Imaging cells and extracellular matrix in vivo by using second-harmonic generation and two-photon excited fluorescence, *Proc. Natl. Acad. Sci. U.S.A. 99*, 11014−11019.

38. Zipfel, W. R., Williams, R. M., Christie, R., Nikitin, A. Y., Hyman, B. T., and Webb, W. W. (2003) Live tissue intrinsic emission microscopy using multiphoton-excited native fluorescence and second harmonic generation, *Proc. Natl. Acad. Sci. U.S.A. 100*, 7075−7080.
39. Stoller, P., Reiser, K. M., Celliers, P. M., and Rubenchik, A. M. (2002) Polarization-modulated second harmonic generation in collagen, *Biophys. J. 82*, 3330−3342.
40. Campagnola, P. J., Wei, M. D., Lewis, A., and Loew, L. M. (1999) High-resolution nonlinear optical imaging of live cells by second harmonic generation, *Biophys. J. 77*, 3341−3349.
41. Bouevitch, O., Lewis, A., Pinevsky, I., Wuskell, J. P., and Loew, L. M. (1993) Probing membrane potential with nonlinear optics, *Biophys. J. 65*, 672−679.
42. Nuriya, M., Jiang, J., Nemet, B., Eisenthal, K. B., and Yuste, R. (2006) Imaging membrane potential in dendritic spines, *Proc. Natl. Acad. Sci. U.S.A. 103*, 786−790.
43. Peleg, G., Lewis, A., Linial, M., and Loew, L. M. (1999) Nonlinear optical measurement of membrane potential around single molecules at selected cellular sites, *Proc. Natl. Acad. Sci. U.S.A. 96*, 6700−6704.
44. Ebrey, T., and Koutalos, Y. (2001) Vertebrate photoreceptors, *Prog. Retinal Eye Res. 20*, 49−94.
45. Palczewski, K. (2006) G protein-coupled receptor rhodopsin, *Annu. Rev. Biochem. 75*, 743−767.
46. Burns, M. E., and Arshavsky, V. Y. (2005) Beyond counting photons: trials and trends in vertebrate visual transduction, *Neuron 48*, 387−401.
47. Lamb, T. D., and Pugh, E. N., Jr. (2004) Dark adaptation and the retinoid cycle of vision, *Prog. Retinal Eye Res. 23*, 307−380.
48. McBee, J. K., Palczewski, K., Baehr, W., and Pepperberg, D. R. (2001) Confronting complexity: the interlink of phototransduction, and retinoid metabolism in the vertebrate retina, *Prog. Retinal Eye Res. 20*, 469−529.
49. Saari, J. C. (2000) Biochemistry of visual pigment regeneration: the Friedenwald lecture, *Invest. Ophthalmol. Visual Sci. 41*, 337−348.
50. Travis, G. H., Golczak, M., Moise, A. R., and Palczewski, K. (2007) Diseases caused by defects in the visual cycle: retinoids as potential therapeutic agents, *Annu. Rev. Pharmacol. Toxicol. 47*, 469−512.
51. Futterman, S., Hendrickson, A., Bishop, P. E., Rollins, M. H., and Vacano, E. (1970) Metabolism of glucose and reduction of retinaldehyde in retinal photoreceptors, *J. Neurochem. 17*, 149−156.
52. Palczewski, K., Jager, S., Buczylko, J., Crouch, R. K., Bredberg, D. L., Hofmann, K. P., Asson-Batres, M. A., and Saari, J. C. (1994) Rod outer segment retinol dehydrogenase: substrate specificity and role in phototransduction, *Biochemistry 33*, 13741−13750.
53. Okajima, T. I., Pepperberg, D. R., Ripps, H., Wiggert, B., and Chader, G. J. (1989) Interphotoreceptor retinoid-binding protein: role in delivery of retinol to the pigment epithelium, *Exp. Eye Res. 49*, 629−644.
54. Qtaishat, N. M., Wiggert, B., and Pepperberg, D. R. (2005) Interphotoreceptor retinoid-binding protein (IRBP) promotes the release of all-trans retinol from the isolated retina following rhodopsin bleaching illumination, *Exp. Eye Res. 81*, 455−463.
55. Batten, M. L., Imanishi, Y., Maeda, T., Tu, D. C., Moise, A. R., Bronson, D., Possin, D., Van Gelder, R. N., Baehr, W., and Palczewski, K. (2004) Lecithin-retinol acyltransferase is essential for accumulation of all-trans-retinyl esters in the eye and in the liver, *J. Biol. Chem. 279*, 10422−10432.
56. Saari, J. C., Bredberg, D. L., and Farrell, D. F. (1993) Retinol esterification in bovine retinal pigment epithelium: reversibility of lecithin:retinol acyltransferase, *Biochem. J. 291*, 697−700.
57. Bernstein, P. S., and Rando, R. R. (1986) In vivo isomerization of all-trans- to 11-cis-retinoids in the eye occurs at the alcohol oxidation state, *Biochemistry 25*, 6473−6478.
58. Jin, M., Li, S., Moghrabi, W. N., Sun, H., and Travis, G. H. (2005) Rpe65 is the retinoid isomerase in bovine retinal pigment epithelium *2*, *Cell 122*, 449−459.
59. Moiseyev, G., Chen, Y., Takahashi, Y., Wu, B. X., and Ma, J. X. (2005) RPE65 is the isomerohydrolase in the retinoid visual cycle, *Proc. Natl. Acad. Sci. U.S.A. 102*, 12413−12418.
60. Redmond, T. M., Poliakov, E., Yu, S., Tsai, J. Y., Lu, Z., and Gentleman, S. (2005) Mutation of key residues of RPE65 abolishes its enzymatic role as isomerohydrolase in the visual cycle, *Proc. Natl. Acad. Sci. U.S.A. 102*, 13658−13663.
61. Simon, A., Hellman, U., Wernstedt, C., and Eriksson, U. (1995) The retinal pigment epithelial-specific 11-cis retinol dehydrogenase belongs to the family of short chain alcohol dehydrogenases, *J. Biol. Chem. 270*, 1107−1112.
62. Yamamoto, H., Simon, A., Eriksson, U., Harris, E., Berson, E. L., and Dryja, T. P. (1999) Mutations in the gene encoding 11-cis retinol dehydrogenase cause delayed dark adaptation and fundus albipunctatus, *Nat. Genet. 22*, 188−191.
63. Crabb, J. W., and Saari, J. C. (1986) The complete amino acid sequence of the cellular retinoic acid-binding protein from bovine retina, *Biochem. Int. 12*, 391−395.
64. Saari, J. C., Nawrot, M., Kennedy, B. N., Garwin, G. G., Hurley, J. B., Huang, J., Possin, D. E., and Crabb, J. W. (2001) Visual cycle impairment in cellular retinaldehyde binding protein (CRALBP) knockout mice results in delayed dark adaptation, *Neuron 29*, 739−748.
65. Mata, N. L., Radu, R. A., Clemmons, R. C., and Travis, G. H. (2002) Isomerization and oxidation of vitamin a in cone-dominant retinas: a novel pathway for visual-pigment regeneration in daylight, *Neuron 36*, 69−80.
66. Thompson, D. A., and Gal, A. (2003) Vitamin A metabolism in the retinal pigment epithelium: genes, mutations, and diseases, *Prog. Retinal Eye Res. 22*, 683−703.
67. Tsina, E., Chen, C., Koutalos, Y., Ala-Laurila, P., Tsacopoulos, M., Wiggert, B., Crouch, R. K., and Cornwall, M. C. (2004) Physiological and microfluorometric studies of reduction and clearance of retinal in bleached rod photoreceptors, *J. Gen. Physiol. 124*, 429−443.
68. Ala-Laurila, P., Kolesnikov, A. V., Crouch, R. K., Tsina, E., Shukolyukov, S. A., Govardovskii, V. I., Koutalos, Y., Wiggert, B., Estevez, M. E. and Cornwall, M. C. (2006) Visual cycle: Dependence of retinol production and removal on photoproduct decay and cell morphology, *J. Gen. Physiol. 128*, 153−169.
69. Chen, C., Tsina, E., Cornwall, M. C., Crouch, R. K., Vijayaraghavan, S., and Koutalos, Y. (2005) Reduction of all-trans retinal to all-trans retinol in the outer segments of frog and mouse rod photoreceptors, *Biophys. J. 88*, 2278−2287.
70. Wu, Q., Chen, C., and Koutalos, Y. (2006) All-trans retinol in rod photoreceptor outer segments moves unrestrictedly by passive diffusion, *Biophys. J. 91*, 4678−4689.
71. Saari, J. C., Garwin, G. G., Van Hooser, J. P., and Palczewski, K. (1998) Reduction of all-trans-retinal limits regeneration of visual pigment in mice, *Vision Res. 38*, 1325−1333.
72. Wu, Q., Blakeley, L. R., Cornwall, M. C., Crouch, R. K., Wiggert, B. N., and Koutalos, Y. (2007) Interphotoreceptor retinoid-binding protein is the physiologically relevant carrier that removes retinol from rod photoreceptor outer segments, *Biochemistry 46*, 8669−8679.
73. Imanishi, Y., Batten, M. L., Piston, D. W., Baehr, W., and Palczewski, K. (2004) Noninvasive two-photon imaging reveals retinyl ester storage structures in the eye, *J. Cell Biol. 164*, 373−383.
74. Imanishi, Y., Gerke, V., and Palczewski, K. (2004) Retinosomes: new insights into intracellular managing of hydrophobic substances in lipid bodies, *J. Cell Biol. 166*, 447−453.
75. Jacobson, S. G., Cideciyan, A. V., Regunath, G., Rodriguez, F. J., Vandenburgh, K., Sheffield, V. C., and Stone, E. M. (1995) Night blindness in Sorsby's fundus dystrophy reversed by vitamin A, *Nat. Genet. 11*, 27−32.
76. Golczak, M., Kuksa, V., Maeda, T., Moise, A. R., and Palczewski, K. (2005) Positively, charged retinoids are potent and selective inhibitors of the trans-cis isomerization in the retinoid (visual) cycle, *Proc. Natl. Acad. Sci. U.S.A. 102*, 8162−8167.
77. Golczak, M., Imanishi, Y., Kuksa, V., Maeda, T., Kubota, R., and Palczewski, K. (2005) Lecithin:retinol acyltransferase is responsible for amidation of retinylamine, a potent inhibitor of the retinoid cycle, *J. Biol. Chem. 280*, 42263−42273.
78. Eldred, G. E., and Katz, M. L. (1988) Fluorophores, of the human retinal pigment epithelium: separation and spectral characterization, *Exp. Eye Res. 47*, 71−86.
79. Parish, C. A., Hashimoto, M., Nakanishi, K., Dillon, J., and Sparrow, J. (1998) Isolation and one-step preparation of A2E and iso-A2E, fluorophores from human retinal pigment epithelium, *Proc. Natl. Acad. Sci. U.S.A. 95*, 14609−14613.
80. Sparrow, J. R., Fishkin, N., Zhou, J., Cai, B., Jang, Y. P., Krane, S., Itagaki, Y., and Nakanishi, K. (2003) A2E, a byproduct of the visual cycle, *Vision Res. 43*, 2983−2990.
81. Mata, N. L., Weng, J., and Travis, G. H. (2000) Biosynthesis of a major lipofuscin fluorophore in mice and humans with ABCR-

mediated retinal and macular degeneration, *Proc. Natl. Acad. Sci. U.S.A. 97*, 7154−7159.
82. Weng, J., Mata, N. L., Azarian, S. M., Tzekov, R. T., Birch, D. G., and Travis, G. H. (1999) Insights into the function of Rim protein in photoreceptors and etiology of Stargardt's disease from the phenotype in abcr knockout mice, *Cell 98*, 13−23.
83. Green, W. R., and Enger, C. (1993) Age-related macular degeneration histopathologic studies. The 1992 Lorenz E. Zimmerman Lecture, *Ophthalmology 100*, 1519−1535.
84. Congdon, N., O'Colmain, B., Klaver, C. C., Klein, R., Munoz, B., Friedman, D. S., Kempen, J., Taylor, H. R., and Mitchell, P. (2004) Causes and prevalence of visual impairment among adults in the United States, *Arch. Ophthalmol. 122*, 477−485.
85. Bindewald-Wittich, A., Han, M., Schmitz-Valckenberg, S., Snyder, S. R., Giese, G., Bille, J. F., and Holz, F. G. (2006) Two-photon-excited fluorescence imaging of human RPE cells with a femtosecond Ti:Sapphire laser, *Invest. Ophthalmol. Visual Sci. 47*, 4553−4557.
86. Han, M., Bindewald-Wittich, A., Holz, F. G., Giese, G., Niemz, M. H., Snyder, S., Sun, H., Yu, J., Agopov, M., La Schiazza, O., and Bille, J. F. (2006) Two-photon excited autofluorescence imaging of human retinal pigment epithelial cells, *J. Biomed. Opt. 11*, 010501.
87. Laing, R. A., Fischbarg, J., and Chance, B. (1980) Noninvasive measurements of pyridine nucleotide fluorescence from the cornea, *Invest. Ophthalmol. Visual Sci. 19*, 96−102.
88. Masters, B. R. (1984) Noninvasive redox fluorometry: how light can be used to monitor alterations of corneal mitochondrial function, *Curr. Eye Res. 3*, 23−26.
89. Davson, H. (1990) *Physiology of the Eye*, 5th ed., Pergamon Press, New York.
90. Maurice, D. M. (1957) The structure and transparency of the cornea, *J. Physiol. 136*, 263−286.
91. Edelhauser, H. F. (2006) The balance between corneal transparency and edema: The Proctor, Lecture, *Invest. Ophthalmol. Visual Sci. 47*, 1754−1767.
92. Piston, D. W., Masters, B. R., and Webb, W. W. (1995) Three-dimensionally resolved NAD(P)H cellular metabolic redox imaging of the in situ cornea with two-photon excitation laser scanning microscopy, *J. Microsc. 178*, 20−27.
93. Masters, B. R., Kriete, A., and Kukulies, J. (1993) Ultraviolet confocal fluorescence microscopy of the in vitro cornea: redox metabolic imaging, *Appl. Opt. 32*, 592−596.
94. Morishige, N., Petroll, W. M., Nishida, T., Kenney, M. C., and Jester, J. V. (2006) Noninvasive corneal stromal collagen imaging using two-photon-generated second-harmonic signals, *J. Cataract Refract. Surg. 32*, 1784−1791.
95. Gatlin, J., Melkus, M. W., Padgett, A., Petroll, W. M., Cavanagh, H. D., Garcia, J. V., and Jester, J. V. (2003) In vivo fluorescent labeling of corneal wound healing fibroblasts, *Exp. Eye Res. 76*, 361−371.
96. Donaldson, P. J., Grey, A. C., Merriman-Smith, B. R., Sisley, A. M., Soeller, C., Cannell, M. B., and Jacobs, M. D. (2004) Functional imaging: new views on lens structure and function, *Clin. Exp. Pharmacol. Physiol. 31*, 890−895.
97. Mathias, R. T., Rae, J. L., and Baldo, G. J. (1997) Physiological properties of the normal lens, *Physiol. Rev. 77*, 21−50.
98. Jacobs, M. D., Soeller, C., Sisley, A. M., Cannell, M. B., and Donaldson, P. J. (2004) Gap junction processing, and redistribution revealed by quantitative optical measurements of connexin46 epitopes in the lens, *Invest. Ophthalmol. Visual Sci. 45*, 191−199.
99. Denk, W., and Detwiler, P. B. (1999) Optical recording of light-evoked calcium signals in the functionally intact retina, *Proc. Natl. Acad. Sci. U.S.A. 96*, 7035−7040.
100. Choi, S. Y., Borghuis, B. G., Rea, R., Levitan, E. S., Sterling, P., and Kramer, R. H. (2005) Encoding light intensity by the cone photoreceptor synapse, *Neuron 48*, 555−562.
101. Yoshida, K., Watanabe, D., Ishikane, H., Tachibana, M., Pastan, I., and Nakanishi, S. (2001) A key role of starburst amacrine cells in originating retinal directional selectivity and optokinetic eye movement, *Neuron 30*, 771−780.
102. Euler, T., Detwiler, P. B., and Denk, W. (2002) Directionally selective calcium signals in dendrites of starburst amacrine cells, *Nature 418*, 845−852.
103. Oesch, N., Euler, T., and Taylor, W. R. (2005) Direction-selective dendritic action potentials in rabbit retina, *Neuron 47*, 739−750.
104. Lukyanov, K. A., Chudakov, D. M., Lukyanov, S., and Verkhusha, V. V. (2005) Innovation: Photoactivatable fluorescent proteins, *Nat. Rev. Mol. Cell Biol. 6*, 885−891.
105. Calvert, P. D., Strissel, K. J., Schiesser, W. E., Pugh, E. N., Jr., and Arshavsky, V. Y. (2006) Light-driven translocation of signaling proteins in vertebrate photoreceptors, *Trends Cell Biol. 16*, 560−568.
106. Schwille, P., Haupts, U., Maiti, S., and Webb, W. W. (1999) Molecular dynamics in living cells observed by fluorescence correlation spectroscopy with one- and two-photon excitation, *Biophys. J. 77*, 2251−2265.
107. Hess, S. T., Huang, S., Heikal, A. A., and Webb, W. W. (2002) Biological and chemical applications of fluorescence correlation spectroscopy: a review, *Biochemistry 41*, 697−705.
108. Maiti, S., Shear, J. B., Williams, R. M., Zipfel, W. R., and Webb, W. W. (1997) Measuring serotonin distribution in live cells with three-photon excitation, *Science 275*, 530−532.
109. Das, T., Payer, B., Cayouette, M., and Harris, W. A. (2003) In vivo time-lapse imaging of cell divisions during neurogenesis in the developing zebrafish retina, *Neuron 37*, 597−609.
110. Morgan, J. L., Dhingra, A., Vardi, N., and Wong, R. O. (2006) Axons and dendrites originate from neuroepithelial-like processes of retinal bipolar cells, *Nat. Neurosci. 9*, 85−92.
111. Dalke, C., and Graw, J. (2005) Mouse mutants as models for congenital retinal disorders, *Exp. Eye Res. 81*, 503−512.
112. Graw, J. (2004) Congenital hereditary cataracts, *Int. J. Dev. Biol. 48*, 1031−1044.
113. Lindsey, J. D., and Weinreb, R. N. (2005) Elevated intraocular pressure and transgenic applications in the mouse, *J. Glaucoma 14*, 318−320.
114. Nemet, B. A., Nikolenko, V., and Yuste, R. (2004) Second harmonic imaging of membrane potential of neurons with retinal, *J. Biomed. Opt. 9*, 873−881.
115. Jester, J. V., Ward, B. R., Takashima, A., Gatlin, J., Garcia, J. V., Cavanagh, H. D., and Petroll, W. M. (2004) Four-dimensional multiphoton confocal microscopy: the new frontier in cellular imaging, *Ocul. Surf. 2*, 10−20.
116. Wang, B. G., and Halbhuber, K. J. (2006) Corneal multiphoton microscopy and intratissue optical nanosurgery by nanojoule femtosecond near-infrared pulsed lasers, *Ann. Anat. 188*, 395−409.
117. Konig, K., Krauss, O., and Riemann, I. (2002) Intratissue surgery with 80 MHz nanojoule femtosecond laser pulses in the near infrared, *Opt. Express 10*, 171−176.
118. Doble, N. (2005) High-resolution in vivo retinal imaging using adaptive optics and its future role in ophthalmology, *Expert Rev. Med. Devices 2*, 205−216.
119. Brakenhoff, G. J., Squier, J., Norris, T., Bliton, A. C., Wade, M. H., and Athey, B. (1996) Real-time two-photon confocal microscopy using a femtosecond, amplified Ti:sapphire system, *J. Microsc. 181*, 253−259.
120. Theer, P., Hasan, M. T., and Denk, W. (2003) Two-photon imaging to a depth of 1000 micron in living brains by use of a Ti:Al2O3 regenerative amplifier, *Opt. Lett. 28*, 1022−1024.
121. Rueckel, M., Mack-Bucher, J. A., and Denk, W. (2006) Adaptive wavefront correction in two-photon microscopy using coherence-gated wavefront sensing, *Proc. Natl. Acad. Sci. U.S.A. 103*, 17137−17142.
122. Denk, W., and Svoboda, K. (1997) Photon upmanship: why multiphoton imaging is more than a gimmick, *Neuron 18*, 351−357.
123. Rodieck, R. W. (1998) *The First Steps in Seeing*, Sinauer Associates, Sunderland, MA.
124. Dowling, J. E. (1987) *The Retina: An Approachable Part of the Brain*, Belknap Press of Harvard University Press, Cambridge, MA.

BI701055G